

# THE IGBT TEST SETUP DESIGN

Master Thesis

By

**Kun Liu**

**Abdirahman Hirsi**

Division of Electric Power Engineering

Department of Energy and Environment

CHALMERS UNIVERSITY OF TECHNOLOGY

Gothenburg, Sweden 2008



# Abstract

An experimental half bridge converter setup is designed in order to explore the switching characteristics and losses of a new type of IGBT module. A specific digital control circuit and a drive circuit for an IGBT are designed and integrated into one PCB which can provide different kinds of precise IGBT gate signals.

The switching characteristics and losses are investigated under different parameters both in a hardware and a simulation. It can be observed that the switching losses are increasing with the increase of voltage and current levels. Increasing the gate resistance also tends to increase the IGBT switching losses, while the reverse recovery losses of the free-wheeling diode decrease. The switching characteristics of the IGBT are not affected by temperature, but the reverse recovery losses increase with the temperature. The stray inductance has a negative effect, since it causes the oscillation both in the voltage and current waveforms.



# Acknowledgements

This thesis work was carried out at the Division of Electric Power Engineering, Department of Energy and Environment of Chalmers University of Technology as part of the Masters Programme in Electric Power Engineering.

The authors would like to thank the following people whose contribution made the thesis succeed. Prof. Torbjörn Thiringer, the supervisor and examiner, for his creative suggestions, constant support and encouragement during this research. PhD student Andreas Karvonen for the design and construction of the control and drive PCB; Robert Karlsson for advice and help with the test circuit; Magnus Ellsén for help in the workshop; Stefan Lundberg for his support; other staff at the department and fellow master students; last but not least, our families and friends for their love and support.



# Table of Contents

<b>Abstract</b>	<b>i</b>
<b>Acknowledgements</b>	<b>iii</b>
<b>Table of Contents</b>	<b>v</b>
<b>1 Introduction</b>	<b>1</b>
1.1 Background . . . . .	1
1.2 Previous work brief introduction . . . . .	3
1.3 Purpose of this thesis . . . . .	4
<b>2 The Theory of IGBT</b>	<b>5</b>
2.1 Structure of the IGBT . . . . .	5
2.2 I-V characteristics . . . . .	6
2.3 Switching characteristics . . . . .	7
<b>3 Experimental Setup Realization</b>	<b>11</b>
3.1 Main converter circuit setup . . . . .	11
3.1.1 Model 1 . . . . .	11
3.1.2 Model 2 . . . . .	14
3.2 Simulation setup . . . . .	16
3.3 IGBT control circuit design . . . . .	19
3.4 IGBT drive circuit design . . . . .	22
3.5 Inductor design . . . . .	24
3.6 Capacitor bank design . . . . .	27
3.7 Heating setup design . . . . .	28
<b>4 Measurements</b>	<b>31</b>
4.1 Voltage measurements . . . . .	31
4.2 Current measurements . . . . .	32

<b>5</b>	<b>Results and Analysis</b>	<b>35</b>
5.1	Control waveform . . . . .	35
5.2	Turn-on transient . . . . .	36
5.3	Turn-off transient . . . . .	39
5.4	Effect of gate resistance . . . . .	41
5.5	Effect of current . . . . .	45
5.6	Effect of temperature . . . . .	46
<b>6</b>	<b>Conclusion and outlook</b>	<b>48</b>
6.1	Conclusion . . . . .	48
6.2	Future work . . . . .	49
	<b>Bibliography</b>	<b>50</b>
<b>A</b>	<b>Control and drive circuit schematics</b>	<b>52</b>

# Chapter 1

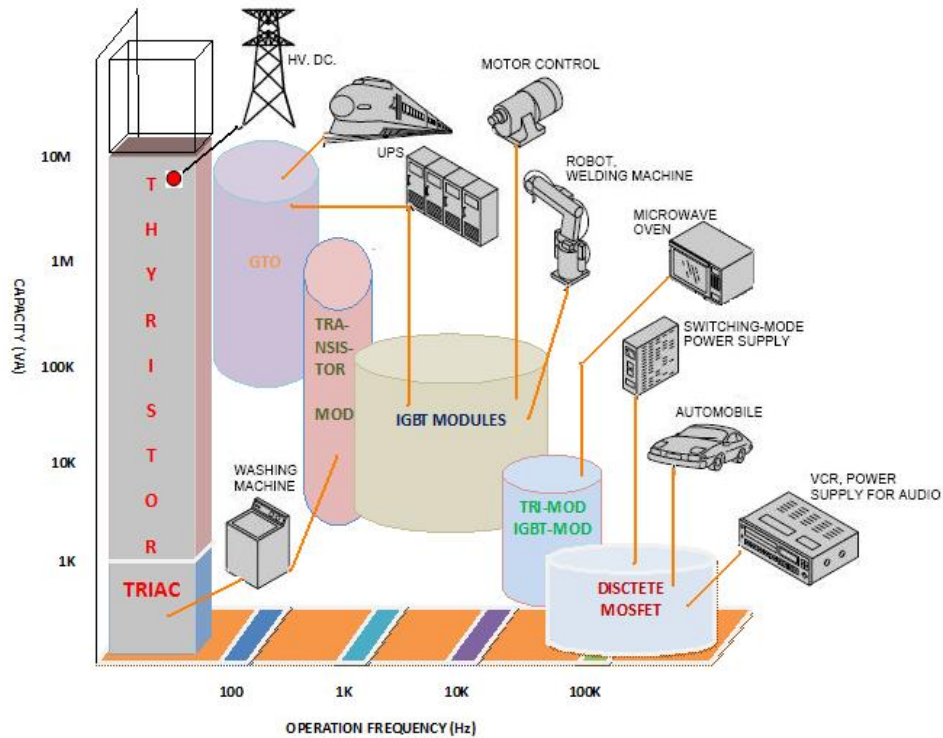
## Introduction

### 1.1 Background

As power conversion today and even more in the future relies more on switch applications, semiconductor manufacturers need to create products that approach the ideal switch. The ideal switch would have: 1) zero resistance or forward voltage drop in the on-state, 2) infinite resistance in the off-state, 3) switch with infinite speed, and 4) would not require any input power to make it switch.

By combining the low conduction loss of a BJT with the switching speed of a power MOSFET an optimal solid state switch would exist. The Insulated-Gate Bipolar Transistor (IGBT) technology offers a combination of these attributes, and IGBT is now beginning to have a major impact on the Power Electronic Systems designed for industrial, consumer applications.

A review of Fig.1.1 indicates that IGBT Modules are expected to take applications where earlier MOSFET Modules and Bipolar Darlington Modules were used, as they will operate in hard switching applications upwards of 20kHz and higher in soft switching applications. Also they serve the lower 1 - 10kHz range previously dominated by Bipolar Transistor modules, up to 1MW applications. Tab. 1 shows

Figure 1.1: *Power Devices Application*

the comparison of switching devices.

Table 1.1: Comparison of switching-device characteristics

Characteristics	MOSFET	IGBT	Bipolar
Drive type	Voltage	Voltage	Current
Drive power	Minimal	Minimal	Large
Drive complexity	Simple	Simple	Medium
Current density for a given voltage drop	High at low voltages, low at high voltages	Very high (small trade-off with switching speed)	Medium (severe trade-off with switching speed)
Switching losses	Very low	Low to medium, depending on trade-off with conduction losses	Medium to high, depending on trade-off with conduction losses

At operating frequencies between 1 and 50 kHz, IGBTs offer an attractive solution over the traditional bipolar transistors, MOSFETs and thyristors. Compared to thyristors, the IGBT is faster, has better  $dv/dt$  immunity and, above all, has better gate turn-off capability. While some thyristors such as GTOs are capable of being turned off at the gate, substantial reverse gate current is required, whereas turning off an IGBT only requires that the gate capacitance be discharged. [1]

Since IGBT has been applied to industry for several decades, the latest generation of IGBTs with rated voltage 6500V and rated current 1200A has been produced and used as power switches in power system.

## 1.2 Previous work brief introduction

In a previous work, a pre-study was done concerning how the voltage level affects the IGBT conduction and switching losses.[2]

In another work [3], a test circuit with a 300V, 40A IGBT was designed. In order to explore the switching characteristics of this IGBT a test system –including a control circuit, a drive circuit and the main test circuit– was built. Furthermore, a current transformer was also designed and constructed to measure the current through the IGBT. Energy losses were investigated under different parameters.

The control circuit, in this work, could not generate well specified control signals, and the drive circuit was separated from the control circuit, which had a negative impact on the control signal to the gate of the IGBT.

### 1.3 Purpose of this thesis

The aim of this thesis is to design and realize an IGBT test setup, to measure and explore the switching characteristics of a new IGBT module (CM300DC-24NFM) with higher rating voltage and current ( $V_{CES}=1200\text{V}$ ,  $I_C=300\text{A}$ ) both in a simulation and a hardware setup. Moreover another vital objective is to design a PCB including a specified digital control circuit and a drive for this IGBT. In addition, an investigation concerning the turn-on and turn-off losses under different gate resistances, load inductances and temperatures are carried out.

# Chapter 2

## The Theory of IGBT

### 2.1 Structure of the IGBT

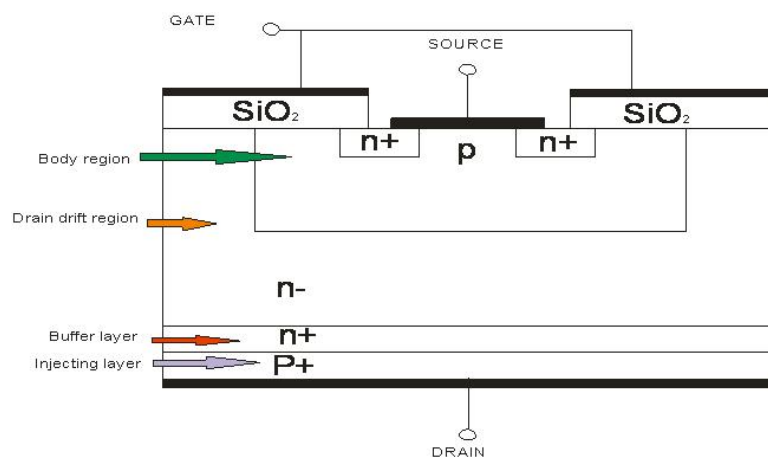


Figure 2.1: *IGBT structure*

As shown in Fig. 2.1 the IGBT structure is similar to that of the vertical diffused MOSFET. The main difference is the p+ layer that forms the drain of the IGBT. This layer forms a PN junction, which injects minority carriers into what would appear to be the drain region of the vertical MOSFET. [4].

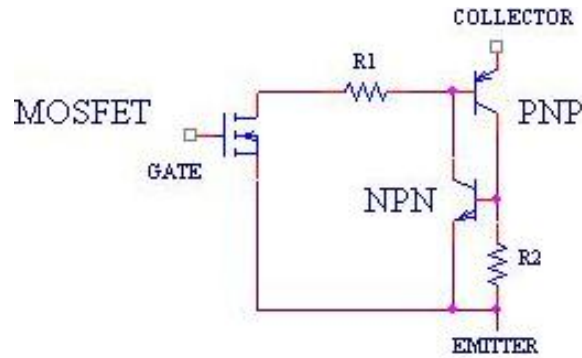


Figure 2.2: IGBT structure resembles as a thyristor (a series of PNPN junctions)

The combination of the NPN and PNP bipolar transistors makes up the parasitic thyristor, as shown in Fig. 2.2. The thyristor can cause the IGBT to latch up which is undesirable turn-on. Latchup can be avoided through the design of the IGBT by optimizing the doping levels and geometries of the various regions shown in Fig. 2.1. In Fig. 2.2,  $R_1$  is the drift region resistance;  $R_2$  is the body region spreading resistance.

## 2.2 I-V characteristics

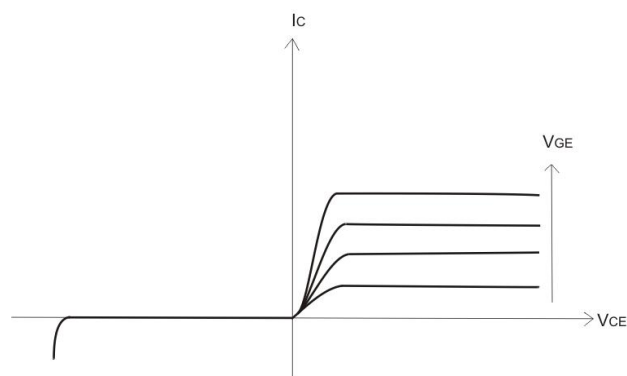


Figure 2.3: I-V Characteristics of IGBT

The I-V characteristics of an n-channel IGBT are shown in Fig. 2.3. In the forward direction the IGBT I-V characteristics are similar to those of a logic-level BJT expect that the controlling parameter is an input voltage ( $V_{GS}$ ), rather than an input current. Since the IGBT is basically a MOSFET, the gate-source voltage controls the state of the device as mentioned in the previous. When  $V_{GS}$  is less than a certain voltage which is called voltage threshold, there is no inversion layer created to connect the drain from the source and hence, the device is in the off state. When  $V_{GS}$  exceeds the threshold, the IGBT is turned to the on-state.[5]

## 2.3 Switching characteristics

### Turn-on

The turn-on switching characteristics for an IGBT transistor are similar to that of a MOSFET. The whole process is indicated in the Fig. 2.4.

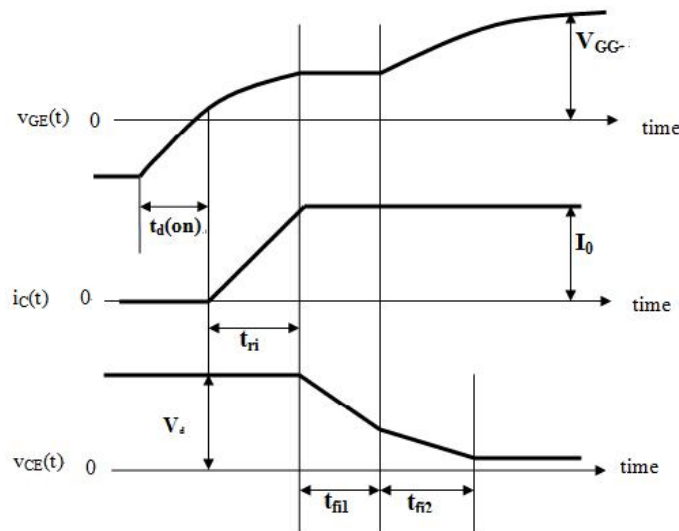


Figure 2.4: IGBT turn-on switching characteristics

As shown in the figure, during the delay time  $t_{d(on)}$  the gate-emitter voltage increases to the threshold voltage  $V_{GE(th)}$  of the device. This is caused by the gate resistance  $R_g$  and the input capacitances ( $C_{GC}$  and  $C_{GE}$ ). But the miller effect capacitance,  $C_{GC}$  is very small that its affect can be neglected. Beyond this time the collector current starts to increase linearly until it reaches to the full load current. During the time when  $i_C=I_0$  the voltage  $V_{GE}$  is first kept constant and at this moment the collector current flows through  $C_{GC}$  only, that causes that the voltage  $V_{CE}$  decreases to the zero on-state. After this moment the voltage  $V_{GE}$  starts to increase until it reaches to  $V_{GG}$ . [6]

Turn-on switching losses: Turn-on switching losses are the amount of total energy losses during turn on under inductive load. It is normally measured from the point where the collector current starts to flow to the point where the collector-emitter voltage drops completely to zero. The turn on energy losses calculation is given by the equation below.

$$E_{loss(on)} = \int_{t_i}^{t_i+t_{on}} v_{CE}(t) i_C(t) dt \quad (2.3.1)$$

where,

$t_i$  is the time when the current starts to rise

$t_{on}$  is the duration for the turn-on transient

### Turn-off

The whole turn-off process is indicated in the Fig. 2.5.

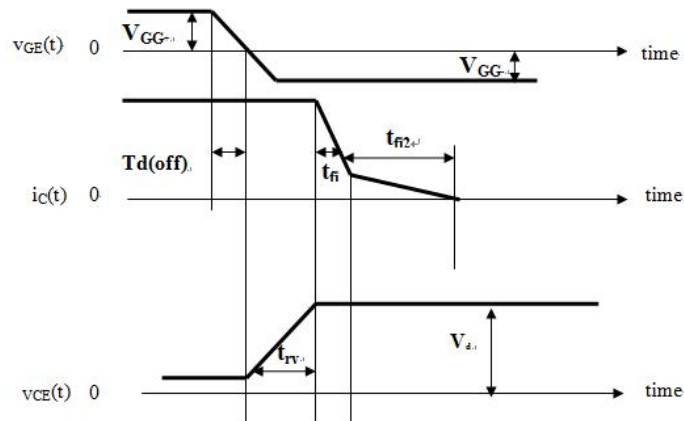


Figure 2.5: IGBT turn-off switching characteristics

The transistor is turned off by removing the gate voltage,  $V_{GE}$ . As shown in the figure, both the voltage  $V_{CE}(t)$  and the current  $i_C(t)$  are kept constant until the gate voltage reaches the voltage  $V_{GE}(I_{on})$  which is used to keep the current  $i_C(t)$  in steady on state. This moment is called the delay off time. After this the collector voltage  $V_{CE}$  starts to increase. The rate of rise for the collector voltage is determined by the gate resistance. When the collector voltage reaches the input voltage the collector current starts to decrease and the free-wheeling diode starts to conduct.[6]

The major difference between the IGBT turn-off and the MOSFET turn-off is observed in the collector current waveform where there are two distinct time intervals. The rapid drop that occurs during the  $t_{f1}$  interval corresponds to the turn-off of the MOSFET section of the IGBT. The 'tailing' of the collector current during the second interval  $t_{f2}$  is due to the stored charge in the n-drift region.[5]

Turn-off switching losses: Turn-off switching are the amount of total energy losses during the turn off under inductive load. It is measured from the point where the collector-emitter voltage begins to rise to the point where the collector current falls

completely to zero. The turn off energy losses calculation is given by the equation below.

$$E_{loss(off)} = \int_{t_v}^{t_v+t_{off}} v_{CE}(t) i_C(t) dt \quad (2.3.2)$$

where,

$t_v$  is the time when the voltage starts to rise

$t_{off}$  is the duration for the turn-off transient

# Chapter 3

## Experimental Setup Realization

In this chapter the working principle of the test setup is first introduced. The simulations of the test circuits are also described. Then the constructions of the components for the experimental test setup are presented.

### 3.1 Main converter circuit setup

#### 3.1.1 Model 1

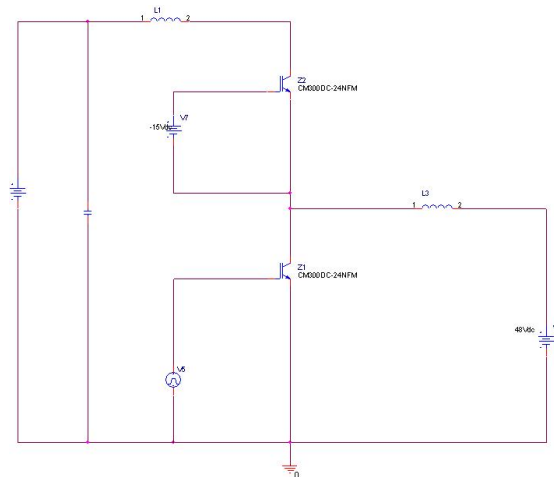


Figure 3.1: *Main test circuit model 1*

Fig. 3.1 shows the main experimental circuit for model 1 which has two IGBTs. During the test process only IGBT1 ( $Z_1$ ) is turned on and off while IGBT2 ( $Z_2$ ) is off all the time. The working process can be divided into 7 stages as shown in Fig. 3.2:

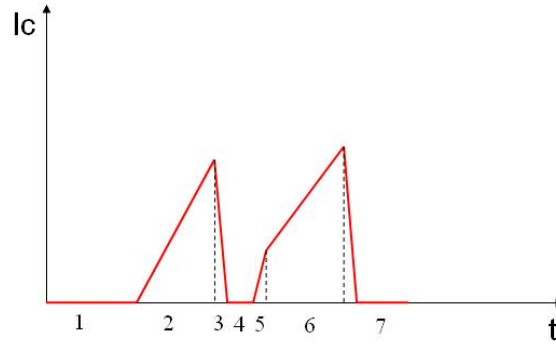
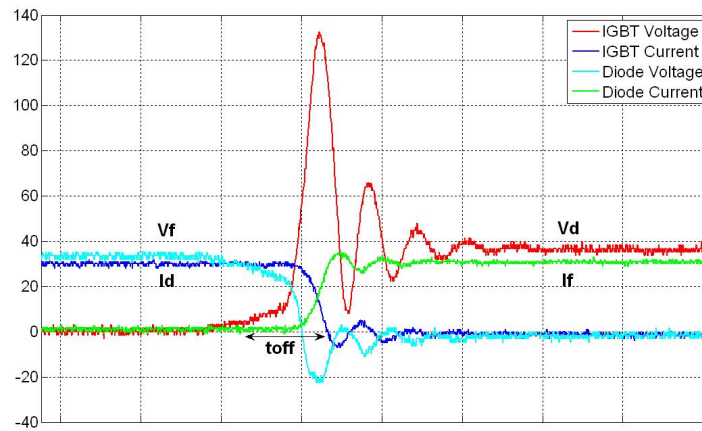
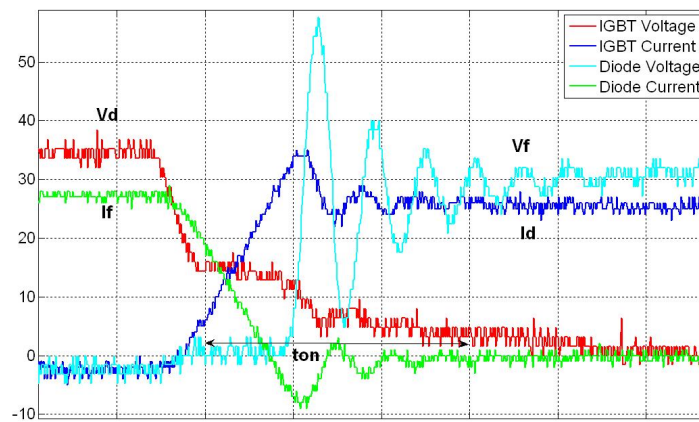


Figure 3.2: *Collector current*

- Stage 1: Before the IGBT1 first turn on.  $v_{CE}=V_6$  (in Fig. 3.1)
- Stage 2: The IGBT1 is turned on for the first time. The current flows from the batteries ( $V_6$  in Fig. 3.1) to the collector of the IGBT1. Because of the load inductance ( $L_3$  in Fig. 3.1), the collector current  $i_C$  increases linearly.
- Stage 3: The IGBT1 is now to be turned off for the first time (as shown in Fig. 3.3). Due to the load inductance the current cannot drop to zero instantaneously, so it is compelled to flow through the free-wheeling diode in the IGBT2 to  $V_1$ . The diode current  $i_f$  increases while  $i_C$  decreases. So that the current through the load inductance  $i_{Ld} = i_C + i_f$ . The collector-emitter voltage  $v_{CE}$  of the IGBT1 increases sharply, and exceeds  $V_1$  because of the stray inductance  $L_1$ , and then drops to  $V_1$ .

Figure 3.3: *The first turn-off, 0.2μs/div*

- Stage 4: The IGBT1 stops conducting completely,  $i_C = 0$ .  $i_{Ld} = i_f, v_{CE} = V_1$ .

Figure 3.4: *The second turn-on, 0.2μs/div*

- Stage 5: The IGBT1 is turned on for the second time (as shown in Fig. 3.4). The current is now compelled to flow through the IGBT1 again.  $i_C$  starts to increase

while the diode current  $i_f$  decreases.  $i_C$  continues to increase until  $v_{CE}$  drops to zero. At this moment, because of the abrupt reverse recovery characteristics of this fast recovery free-wheeling diode,  $i_C$  starts to oscillate until  $i_f$  drops to zero.

- Stage 6: The IGBT1 is turned on completely. It is the same process as stage 2.
- Stage 7: The IGBT1 is turned off for the second time.

The turn-off and turn-on characteristics of the IGBT are measured and investigated at stage 3 and 5.

### 3.1.2 Model 2

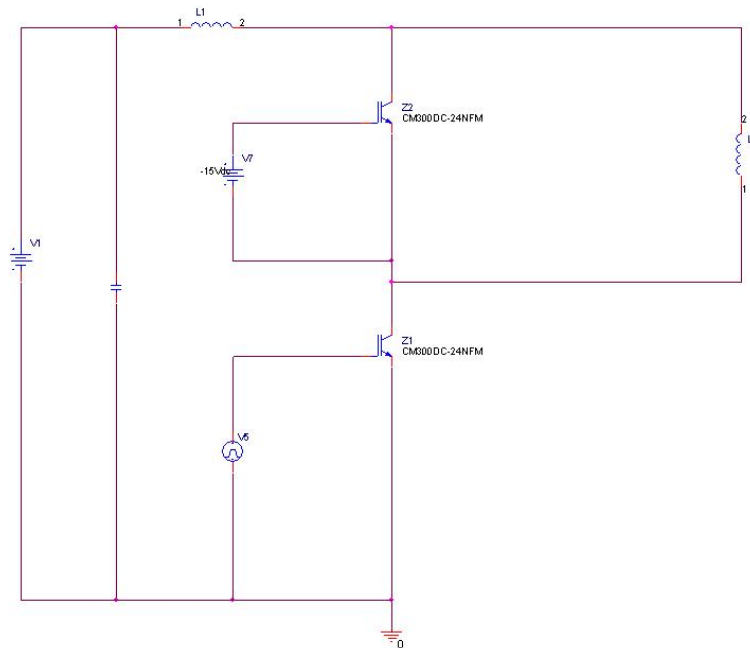


Figure 3.5: Main test circuit model 2

Fig. 3.5 shows the main circuit of model 2. The main difference between the model 2 and model 1 is stage 4. In model 2 when the IGBT1 is turned off, the current will start free-wheeling through the diode in the IGBT2 and the load inductance  $L_3$ .

The switching characteristics of the IGBT and the free-wheeling diode are shown in Fig. 3.6 and 3.7

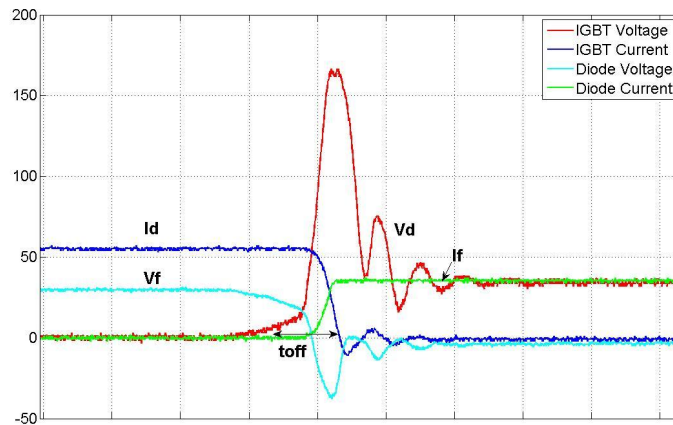


Figure 3.6: *The first turn-off,  $0.2\mu\text{s}/\text{div}$*

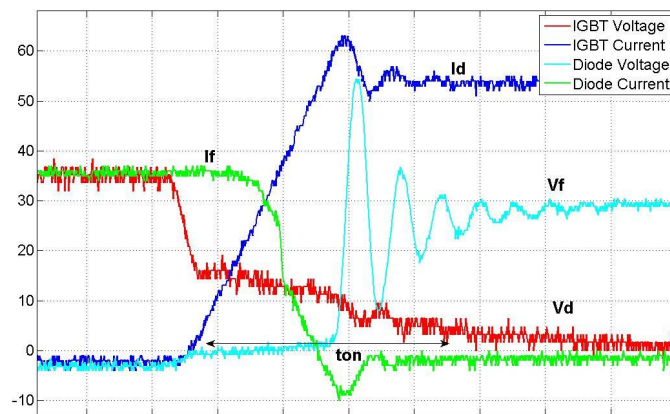


Figure 3.7: *The second turn-on,  $0.2\mu\text{s}/\text{div}$*

Compared with the figures (3.3) and (3.4), it can be seen that the turn-off and turn-on transients of model 2 are almost consistent with model 1.

Fig. 3.8 shows the hardware circuit setup.

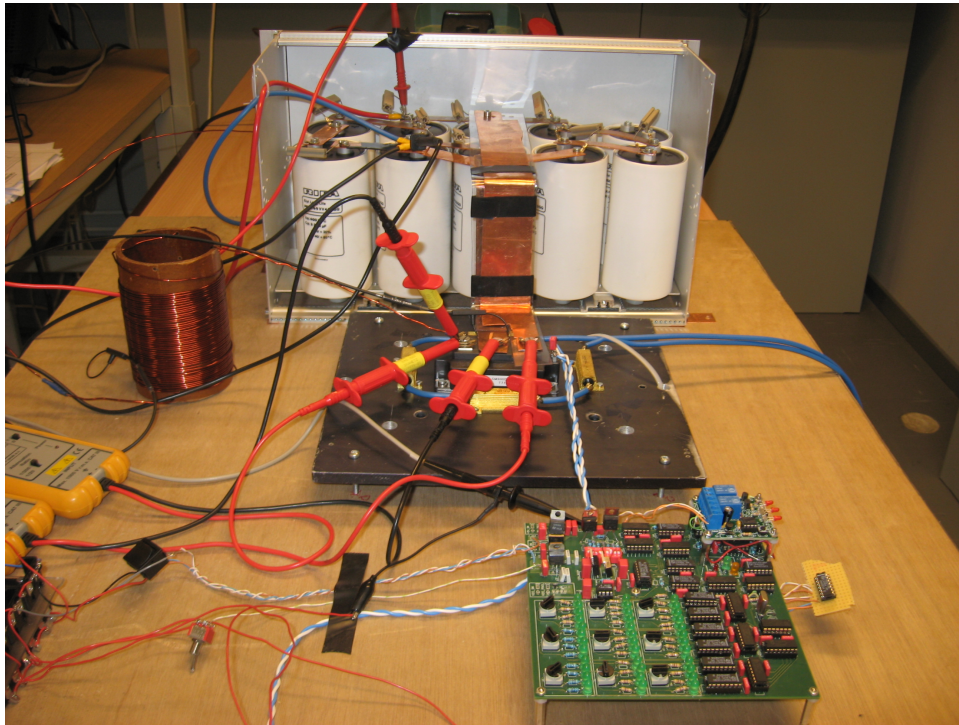


Figure 3.8: *Main test setup*

## 3.2 Simulation setup

Since a simulation is the first step to build a hardware setup. In this project the Program *Cadence*<sup>®</sup> *Orcad*<sup>®</sup> 16.0 is used as the simulation platform .

The hardware IGBT module is *MITSUBISHI*<sup>®</sup> CM300DC-24NFM. The main parameters of this module are listed in Tab. 3.1.

Table 3.1: IGBT module used in simulation and hardware

<b>Rated Voltage <math>V_{CE}</math> (V)</b>	1200
<b>Rated Current <math>I_C</math> (A)</b>	300
<b>Rise Time <math>t_r</math> (ns)</b>	80
<b>Fall Time <math>t_f</math> (ns)</b>	200
<b>Diode Reverse Recovery Time <math>t_{rr}</math> (ns)</b>	180

Since the module is a new generation, the model was not available in the *Pspice*<sup>®</sup> library. So a new model which is based on the parameters of CM300DC-24NFM should be created in the Pspice Model Editor. Four groups of parameters are needed to create a new IGBT model in the Pspice. Three of them are fall time, saturation characteristics and gate charge which could be gotten from the IGBT datasheet. For the last group, transfer characteristics, which is not included in the datasheet, a measurement circuit is built to acquire these characteristics, and the characteristics curve is plotted as shown in Fig. 3.9.

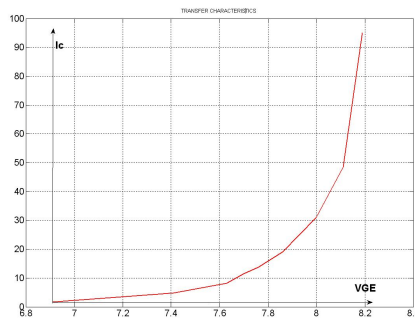


Figure 3.9: IGBT transfer characteristics

The simulation circuits for model 1 and model 2 are shown in Fig. 3.10 and 3.11. It can be seen that a separate diode is added in anti-parallel with the IGBT module since the free-wheeling diode is not included in the Pspice IGBT library.

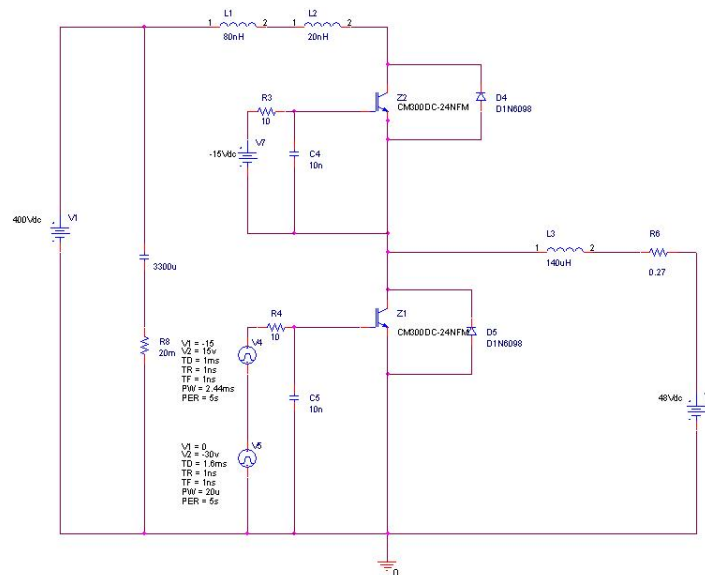


Figure 3.10: Model 1 simulation

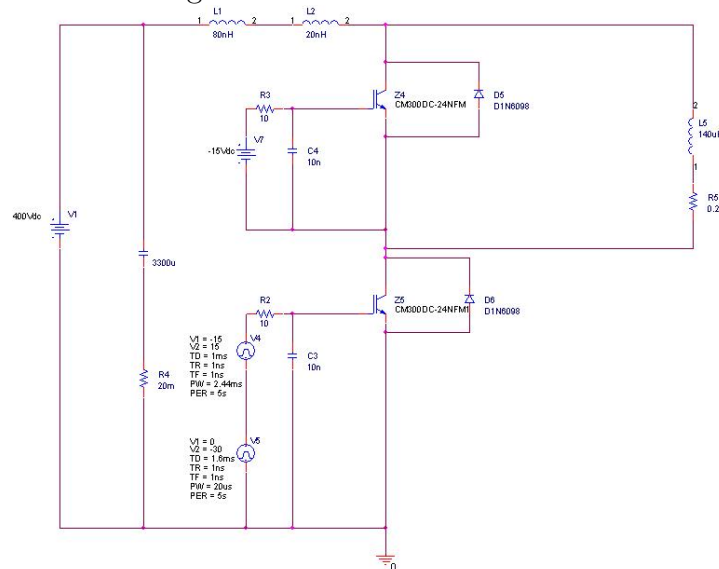


Figure 3.11: Model 2 simulation

### 3.3 IGBT control circuit design

The digital control circuit in this project is designed to obtain the specified durations of stage 2, 4 and 6 which are deliberated in the previous section.

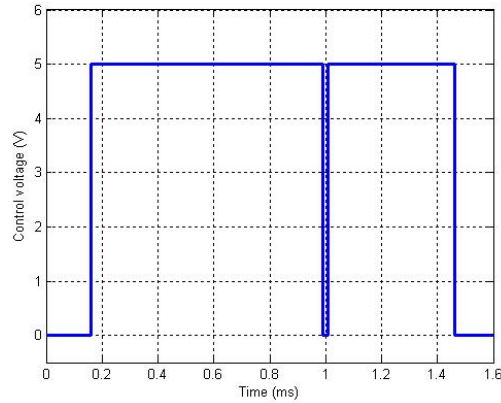


Figure 3.12: *Control waveform*

In Fig. 3.12 a control waveform which has 2 positive pulses (corresponding to stage 2 and 6 in Fig. 3.2) and a short interval (corresponding to stage 4) between them is generated. The design purpose of this control waveform is to turn on and turn off the IGBT twice. Fig. 3.13 illustrates the main parts of the control circuit.

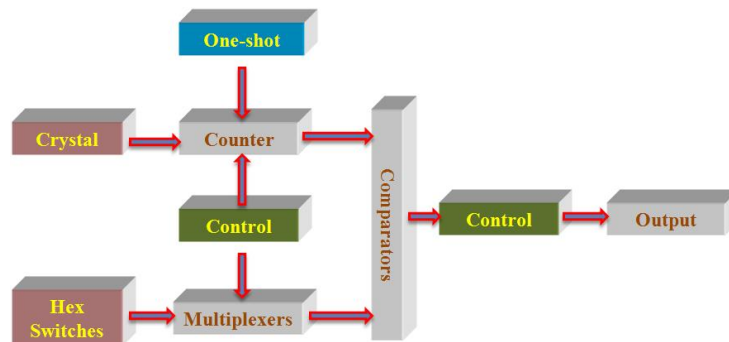


Figure 3.13: *Control circuit schematics*

The working principle of the control circuit:

The lengths of stage 2, 4 and 6 are set by the hex rotary switches. Three hex rotary switches generate one stage duration, and decode these three hex signals to 12 bits binary signals. After decoding, these 12 bits signals are transmitted to 6 dual 4-input multiplexers, and then transmitted to the comparators to compare with the 12 signals from the counter.

When the control switch is on, a one-shot signal is generated by the one-shot circuit part to trigger the counter. So that the counting of the first stage (stage 2) starts.

A 3.2768MHz crystal (can be replaced by other frequency crystals) is used as an oscillator to provide a circuit clock signal. This signal is then transferred to a 12-stage counter, and is divided into 12 binary signals with different frequencies by this counter. These 12 bits signals are allocated to 3 groups with 4 adjacent bits in each group that are called low 4 bits, medium 4 bits and high 4 bits signals respectively. After that each group of the signals are transmitted to one magnitude comparator, and are compared with another group of signals from a multiplexer. These three magnitude comparators are connected in cascading. In other words, the signal from the crystal is compared with the signals from the three hex rotary switches. When each signal from the counter equals to the corresponding signal from the multiplexer, the "equal output" of the third comparator (Fig. 3.14) will generate a high level signal. This signal means that the counting of stage 2 has finished, and the duration of stage 4 will start to count. In the same way, after finishing the counting of stage 4, another high level signal is generated by the third comparator, so that the stage 6 starts to be counted. When the counting of stage 6 is finished, a signal will be sent

to the counter to count no more. The "equal output" will be sent to the last part of the control circuit to generate the control waveform in Fig. 3.12.

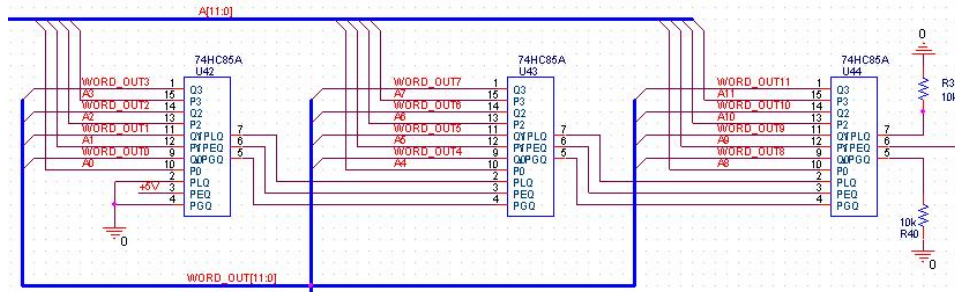


Figure 3.14: Three comparators in cascading

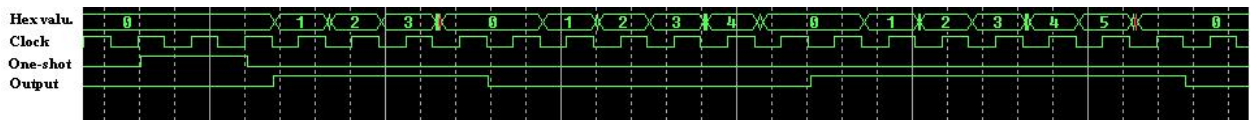


Figure 3.15: Control circuit time sequence diagram

Fig. 3.15 is an example which illustrates how this control circuit works: first the hex switches are set to the values (stand for the duration of stage 2, 4 and 6) that the test operator wants. In Fig. 3.15 the values of the nine hex switches are set to 0-0-3, 0-0-4 and 0-0-5 respectively. These correspond to four periods, five periods and six periods (counting from zero) of the clock signal from the crystal oscillator. This means that the duration of stage 2 is four periods of the oscillator signal; the duration of stage 4 is five periods of the oscillator signal; the duration of stage 6 is six periods of the oscillator signal. So the duration of stage 2, 4 and 6 should have the exact same length as set by the hex switches.

Considering the safety reasons, it is a good idea to use remote controller to trigger the IGBT control circuit. 2-CHANNEL IR REMOTE TRANSMITTER and

2-CHANNEL IR REMOTE RECEIVER (as shown in Fig. 3.16) are used in this project, so that the test operator can control the system switch on and off from a long distance, avoiding to touch the control board when the system is working.

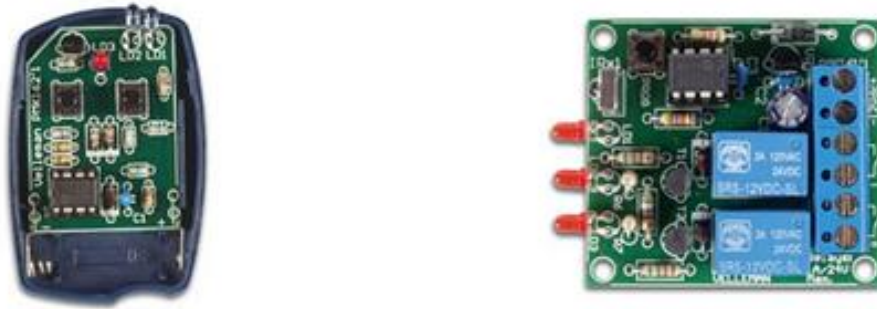


Figure 3.16: *Remote transmitter and receiver*

### 3.4 IGBT drive circuit design

The IGBT gate drive circuit is the bridge between the control circuit and the IGBT, it is also the key point for the IGBT system design. Normally the IGBTs are used as power switches, so that they can turn on and off as fast as possible to minimize the power losses. This means that the drive circuit of the IGBT should have a high performance to drive the IGBT.

The IGBT gate drive conditions are closely related to the static and dynamic characteristics of the IGBT. For the drive circuit design, the forward/reverse bias voltage, the gate resistance  $R_g$  in the drive circuit and the capacitance  $C_{GE}$  between the gate and the emitter of the IGBT should be considered, due to the fact that they greatly affect the IGBT on-state voltage, switching losses, capability of bearing

short-circuit and so on. Mistrigger caused by  $dU_{GS}/dt$  should also be avoided. The IGBT gate drive circuit is shown in Fig. 3.17.

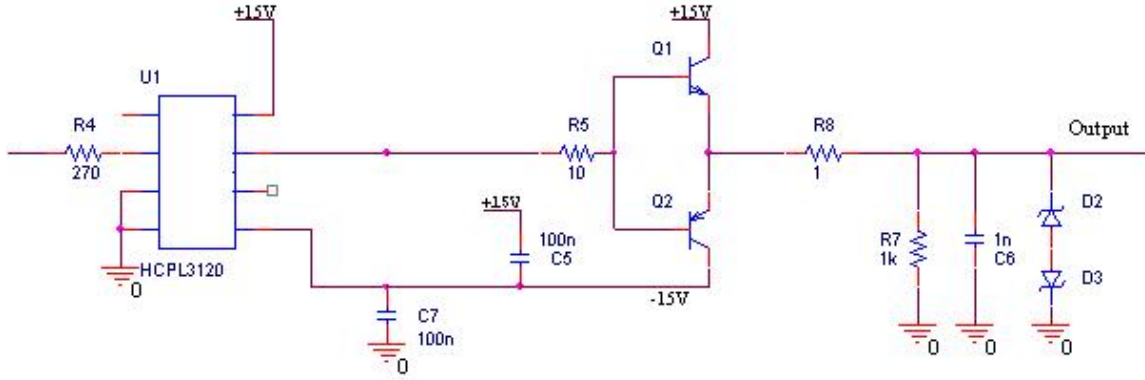


Figure 3.17: IGBT drive circuit

The IC HCPL-3120 used in this drive circuit is a typical IGBT gate drive optocoupler. It has 15 kV/ms Minimum Common Mode Rejection (CMR) at  $V_{CM} = 1500$  V, which is suitable for the IGBT working conditions. The output current from HCPL-3120 is only 2 Amp, this should be amplified by a push-pull amplifier to a higher current level to turn on the IGBT more faster. Suppose that the gate current is 20 Amp,

$$R_g = \frac{V_{GS} - V_{EE} - 1 - V_{OL}}{I_g} = \frac{15 - (-15) - 1 - 2}{20} = 1.35\Omega \quad (3.4.1)$$

During the test different gate resistors  $R_g$  are applied to investigate the effect of  $R_g$  to the IGBT switching characteristics. Furthermore, the  $\pm 15$ V bias voltages also support to turn the IGBT on and off quickly and completely. At the point of drive output, a resistor ( $R_7$  in Fig. 3.9) is added to restrict overvoltage between the gate and emitter of the IGBT, a capacitor ( $C_6$ ) is used to reduce  $di_c/dt$ , and two Zener

diodes ( $D_2$  and  $D_3$ ) are used to restrict the high peak voltage of the output.

In order to obtain a precise IGBT gate signal the control and drive circuit in this project are integrated into one PCB, as shown in Fig. 3.18.

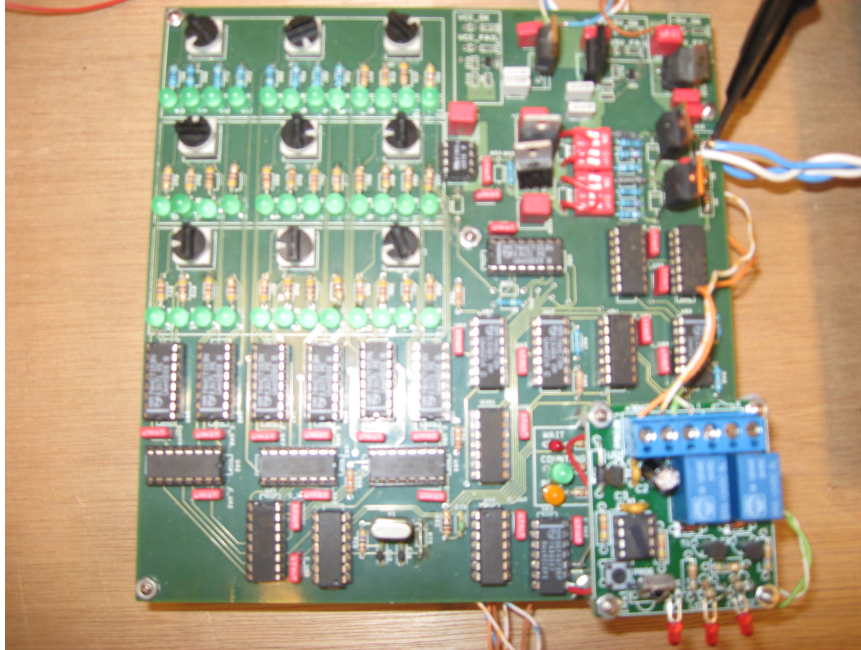


Figure 3.18: *Control and drive PCB*

### 3.5 Inductor design

The load inductor used in the main circuit is designed and constructed in this project. Certain parameters, such as the maximum current that flows in the circuit should be considered in the inductor design. However, the current duration in the main circuit is less than 2 milliseconds so that the effect of the dimensions of the copper wire needs not to be considered from a thermal point of view. Furthermore, in order to minimize the effects of the inductor resistance to the current through the inductor,

the wire (conductor) should have a larger diameter.

Considering the complicity and cost, an air core inductor is constructed. The picture of the constructed inductor is shown in Fig. 3.19.



Figure 3.19: *The constructed inductor*

$$L = \frac{r^2 N^2}{9r + 10l} \quad (3.5.1)$$

where,

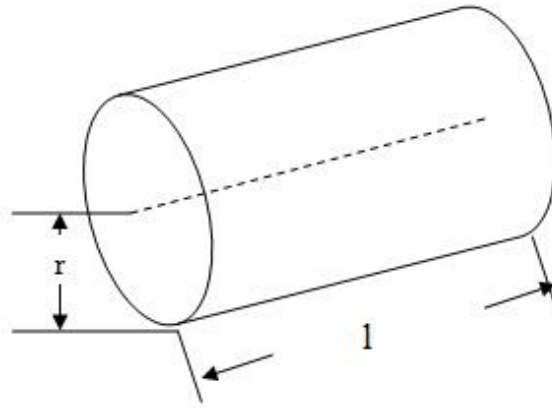
L is inductance in  $\mu\text{H}$

r is the outer radius of coil in inches

l is the length of coil in inches

N is the number of turns

Formula 3.5.1 is used to decide the parameters of the air core inductor (Fig. 3.20 illustrates the dimensions of the air core inductor):

Figure 3.20: *The air core inductor dimensions*

In the simulation the inductance is chosen to be  $130 \mu\text{H}$ , so the other parameters are calculated by using (3.5.1) and the results are listed in Table 3.2. Across the parameters, a copper conductor AWG 18 with a diameter of 1.02mm is selected.

Table 3.2: The parameters of the inductor

Coil Diameter (mm)	Coil Length (mm)	Turns	Tube Length
90	120	52	132

The length of the copper wire:  $l_{cond}=2\pi rN=2\pi \cdot 0.045 \cdot 52=14.7\text{m}$

The mass of copper wire:  $m=7.32 \cdot 0.0147=0.108\text{kg}$

The resistance of the copper wire:  $R=21 \cdot 0.0147=0.310\Omega$

The inductance value can also be measured by RCL meter. Here *Philips*<sup>®</sup> PM 6303 RCL meter is used and it indicates that the measured inductance value is  $139.3\mu\text{H}$ .

### 3.6 Capacitor bank design

A capacitor bank that is used in the main circuit is constructed in this project, due to that the capacitor with 1200V rating voltage was not available in the laboratory. As shown in Fig. 3.21, all capacitors are  $3300\mu\text{F}$  with rated 400V voltage, so there should be 3 capacitors in series in one column and 3 columns in parallel to satisfy the 1200V voltage request and still keep a good capacitance value.

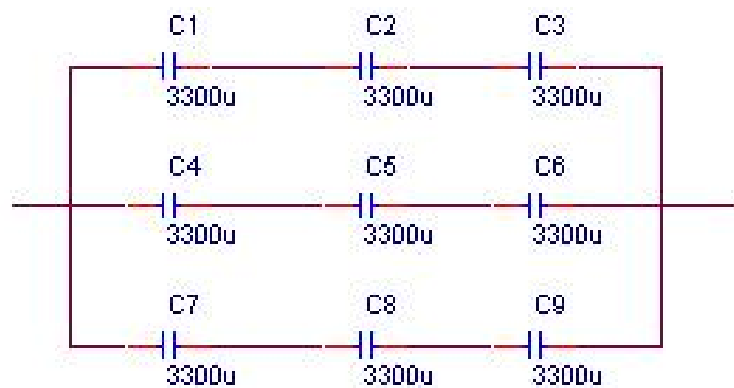


Figure 3.21: *The capacitor bank schematics*

One point that needs to be emphasized here is the inductance generated by the connections from the IGBT to the capacitor bank. This stray inductance ( $L_1$  as shown in Fig. 3.1 ) will affect the test circuit strongly when the IGBT is turned on at the second time. In this aspect, the inductance should be as small as possible. To realize this, the connection wires [7] are replaced by two copper sheets[8], as shown in Fig. 3.22, to reduce the stray inductance between them. A high dielectric strength mylar plastic plate is added between the copper sheets to provide insulation. An alternative approach to reduce the stray inductance is using an RCD snubber as a clamp, as shown in Fig. 3.23. [9]



Figure 3.22: *The constructed capacitor bank*

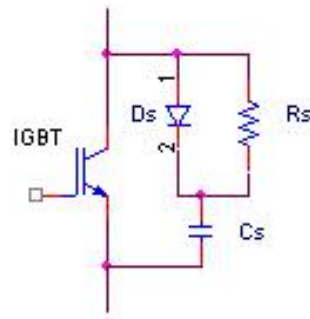


Figure 3.23: *RCD snubber*

### 3.7 Heating setup design

The ambient temperature is an important factor which will affect the operation of the IGBT greatly. For the purpose of testing the IGBT in different temperatures, a

heating setup is integrated into the main system. Here power resistors are used as the heating setup, which are designed and manufactured to handle more power with respect to their size than other resistors types.

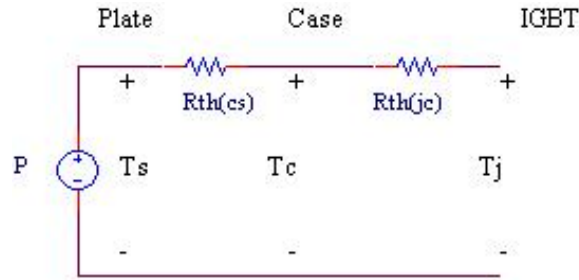


Figure 3.24: *Equivalent circuit of the heat flow based on the thermal resistance*

Regarding Fig. 3.24, if the temperature of the aluminum plate is measured, then the IGBT temperature can be calculated using

$$T_j = T_s - P(R_{th(cs)} + R_{th(jc)}) \quad (3.7.1)$$

where,

$T_s$  is the temperature of plate

$T_j$  is the temperature of IGBT junction

$P$  is the power dissipated by power resistors to the aluminum plate

$R_{th(cs)}$  is the case-to-plate thermal resistance

$R_{th(jc)}$  is the junction-to-case thermal resistance

The thermal resistances are obtained from the IGBT datasheet:  $R_{th(cs)}=0.035^\circ\text{C}/\text{W}$ ,  $R_{th(jc)}=0.06^\circ\text{C}/\text{W}$ .

The heating setup is composed of four power resistors which are mounted around the IGBT module. Both the IGBT and the heating setup are placed on the same aluminum plate. The model of the resistors are of *ARCOL*<sup>®</sup> HS50 1R, see Fig. 3.25

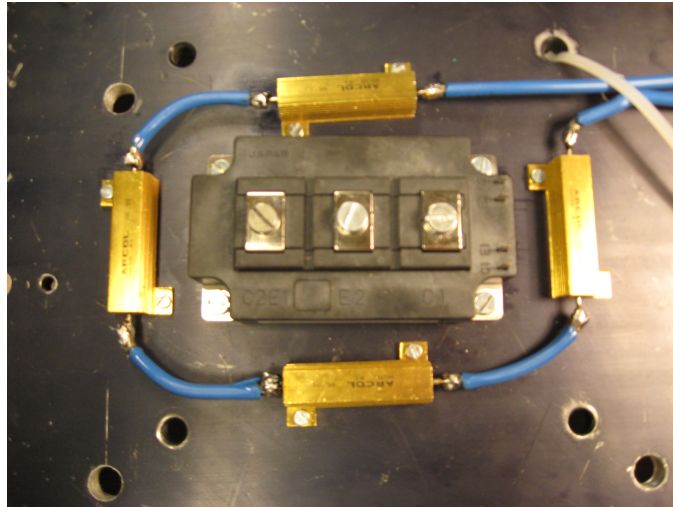


Figure 3.25: *The constructed heating setup*

In reality, it is difficult to calculate how much thermal energy is transferred to the aluminum plate from power resistors. In point of fact only a small fraction of total heat is transferred to the aluminum plate. So in order to simplify the calculations, the temperature of the IGBT is assumed to be the same as the aluminum plate.

# Chapter 4

## Measurements

Accurate measurements depend on accurate equipment and robust connections. Poor connections and noise picked up through unshielded leads and improperly grounded circuits will certainly yield inaccurate data. Packaged sensors are typically designed to ensure accurate output signals with proper component placement, shielding, filtering, and bypassing power and ground I/O connections. Unprotected sensors, however, such as thermocouples and strain gages are often exposed to numerous types of noise signals that can couple into the sensors and leads and contaminate the desired signal. Those who install such sensors must follow industry-accepted practices to ensure that the sensors' output signals are reliable, unbiased, and free of noise and interference.

### 4.1 Voltage measurements

The differential techniques employed permit measurements to be taken between two points in a circuit without reference to ground. This allows the oscilloscopes to be safety grounded without the use of opto-isolators or isolating transformers. While a matched pair of single-ended probes can be used, a true differential probe typically gives higher performance, providing high Common Mode Rejection Ratio (CMRR),

broad frequency range, and minimal time skew between inputs. Differential signaling eliminates common mode noise, it also reduces the need for a common reference voltage between the transmitter and the receiver against which the signal is compared to determine its logic level, eliminating some signal integrity issues such as "ground bounce".[10][11]

An issue with high-frequency probes is the repeatability of measurements made with the probe. Ideally, probe, cable, and hand position should not cause variations in probe measurements. Unfortunately, however, these factors often affect the measurement, usually because of variation in the outside-mode impedance. This impedance is more complex than the probe models show because of the unshielded transmission line (or antenna) that probe, hand, and cable positions can greatly affect. Analysis of the differential model with variation in the outside-mode impedance shows that this variation causes little change in the response.

In this project, *theLeCroy*<sup>®</sup> AP032 differential active probe is used to measure voltages. The differential capability of this probe allows measurements to be made between two points in a circuit without reference to ground. The two input signals are processed inside the probe and the resulting single-ended signal may be measured by any grounded oscilloscope.

## 4.2 Current measurements

Voltage drops are relatively easy to measure with most instruments because the difference in voltage appears between any two points in a circuit. By comparison, simple direct-connection current measurements are more troublesome, because the current

appears within a loop and the loop must be opened to insert the ampermeter. Moreover, the ampermeter contains a characteristic resistance or impedance that most often changes the circuit parameters and must be compensated to obtain accurate measurements. Tab. 4.1 summaries the different current measuring methods.[12]

Table 4.1: Comparison of current measuring methods

	Coaxial Shunt	CT	Hall Effect Devi.	Rogowski Coil
Isolation	Worst	Best	Best	Best
Weight	Worst	Moderate	Moderate	Best
DC Response	Best	Worst	Best	Worst
Low Freq. Response	Best	Moderate	Best	Best
High Freq. Response	Best	Moderate/Best	Moderate	Best
Output	Voltage	Current	Voltage	Voltage
Ease of Installation	Worst	Moderate	Moderate	Best
Cost	Worst	Moderate	Moderate	Best

Rogowski coil can measure large currents without saturating, are easy to use, non-intrusive and have a very wide bandwidth. It also provides an isolated measurement at ground potential and measure fast changes of current. However, the self-capacitance and self-inductance of the coil cause a resonance. The resonant frequency is an important parameter of a Rogowski coil and is crucial to an understanding of its high-frequency behavior.

By comparing the current transformer, the Rogowski coil has following advantage:

- Do not suffer from magnetic saturation

- Can take large current overloads without damage
- Can measure very large currents without increasing in transducer size
- Have a very wide bandwidth (although this is also true for certain specialized CTs)
- Are flexible, thin, clip-around and easy to use

# Chapter 5

## Results and Analysis

In this chapter the obtained experimental results and the energy losses calculated from them are presented. Factors which affect the switching losses including: turn-on and turn-off transient times, voltage and current levels, gate resistances and temperatures are investigated. All the data both measured and simulated are from model 1, due to the range of measurement equipments.

### 5.1 Control waveform

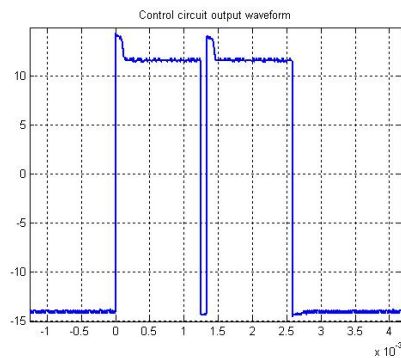


Figure 5.1: *control waveform from hardware*

The measured control signal from Fig.5.1 is composed of 2 pulses and a short off duration between them. The spikes that appear at the beginning of the 2 pulses are caused by the stray inductance of the control PCB. Moreover the length of the 2 pulses and the off duration are exactly the same as those set by hex rotary switches.

## 5.2 Turn-on transient

### IGBT

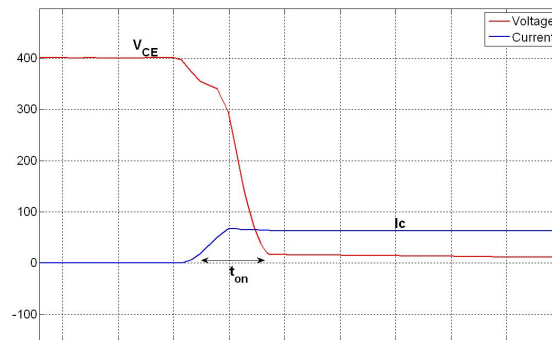


Figure 5.2: *Simulated turn-on transient,  $0.2\mu\text{s}/\text{div}$*

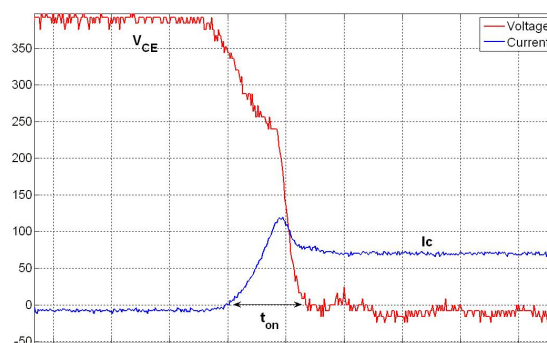


Figure 5.3: *Measured turn-on transient,  $0.2\mu\text{s}/\text{div}$*

It can be seen from Fig. 5.2 and 5.3 that the simulated turn-on transient of the IGBT is consistent with the measured one. However, the measured turn-on durations for 36V  $V_{CC}$  (Fig. 3.4) are much longer compared with the 400V ones from Fig. 5.3. This is because of the  $V_{CE}$ -tail characteristics of the IGBT modules. This voltage tail effect decreases with the increasing of the  $V_{CE}$ . A slow discharging of  $C_{GC}$  (gate-collector capacitance) causes the long  $V_{CE}$ -tail. An approach to solve this problem is to add an RC-network in the gate drive circuit, as shown in Fig. 5.4 [13]

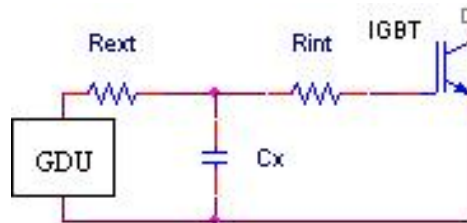


Figure 5.4: Gate drive circuit with an extra RC

The negative current that appears in the measured turn-on transient is caused by the Rogowski coil, this can be eliminated by adding a correspondent plus gain.

### Free-wheeling diode

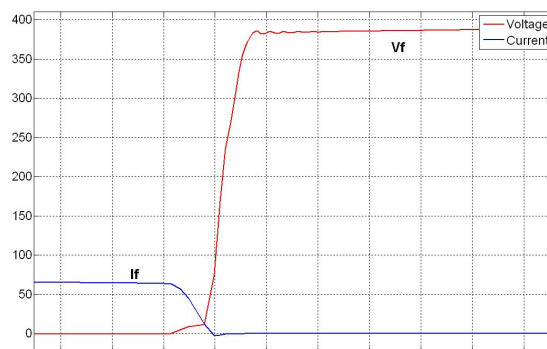


Figure 5.5: Simulated diode voltage and current,  $0.2\mu\text{s}/\text{div}$

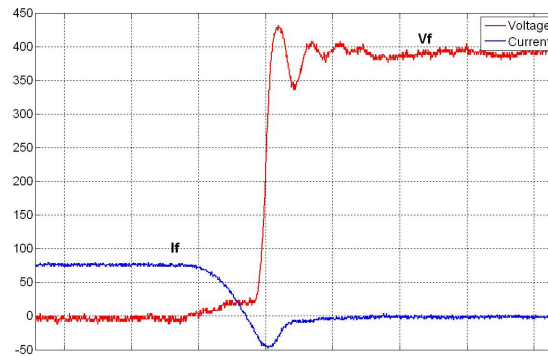


Figure 5.6: Measured diode voltage and current,  $0.2\mu\text{s}/\text{div}$

At the moment of the IGBT turn-on, the free-wheeling diode in the other IGBT stops conducting, as shown in Fig. 5.5 and 5.6. There are no reverse recovery characteristics in the simulated turn-off transient of the free-wheeling diode, this is due to that the free-wheeling diode is not integrated into the IGBT module in the Pspice. The separate schottky diode, which is used in the simulation, is not the same model as the one in the hardware .

## 5.3 Turn-off transient

### IGBT

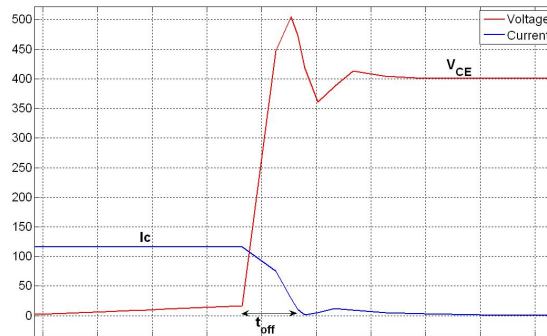


Figure 5.7: *Simulated turn-off transient, 0.2 $\mu$ s/div*

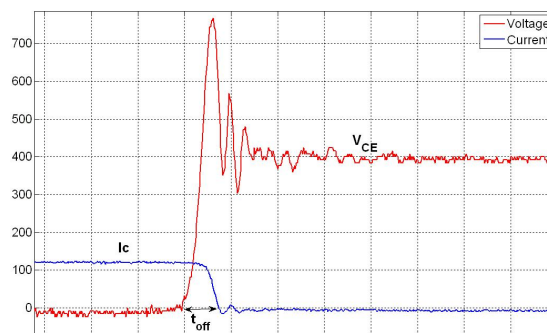


Figure 5.8: *Measured turn-off transient, 0.2 $\mu$ s/div*

Both the simulated and the measured collector-emitter voltage  $V_{CE}$  oscillate at the turn-off duration, as shown in Fig. 5.7 and 5.8. This can be caused by the reverse-recovery characteristics of the free-wheeling diode in the other IGBT. The difference of the free-wheeling diode in the simulation and hardware setup make the oscillation

frequency inconsistent. The voltage spike in the simulation is not coinciding with the one in the hardware measurement; the reason is that the values of the stray inductances in the simulation and the hardware are not exactly the same.

### Free-wheeling diode

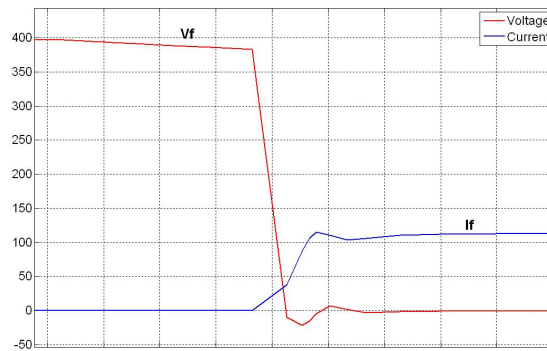


Figure 5.9: *Simulated diode voltage and current,  $0.2\mu\text{s}/\text{div}$*

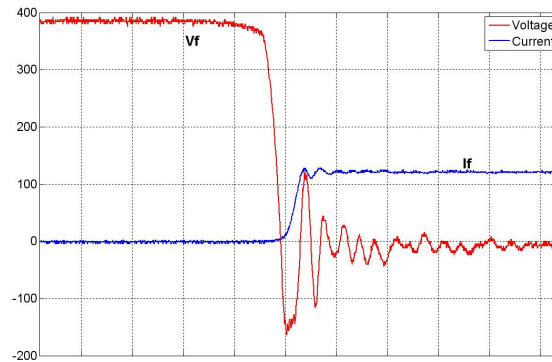


Figure 5.10: *Measured diode voltage and current,  $0.2\mu\text{s}/\text{div}$*

From Fig. 5.10, it can be seen that there are almost no losses during the diode turn on. According to this, only the the free-wheeling diode reverse recovery losses

are investigated in the following analysis.

## 5.4 Effect of gate resistance

### IGBT

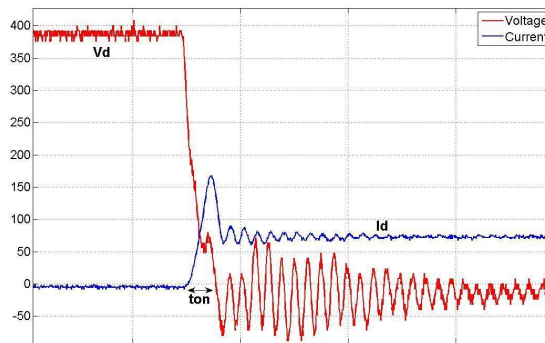


Figure 5.11: Measured turn-on transient,  $R_g=2.667\Omega$ ,  $0.5\mu s/div$

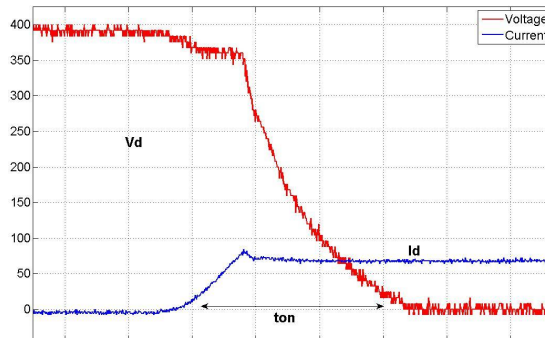


Figure 5.12: Measured turn-on transient,  $R_g=40\Omega$ ,  $0.5\mu s/div$

A small gate resistance charges and discharges the IGBT input capacitance faster which reduces the switching times and switching losses and improves immunity to

dv/dt during turn-on. However, a small gate resistance can lead to oscillations between the IGBT input capacitance and the parasitic lead inductance, as shown in figures 5.11 and 5.12.

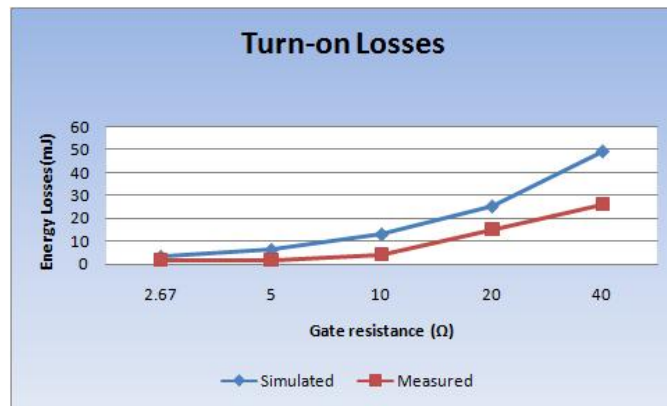


Figure 5.13: Turn-on losses for different gate resistances

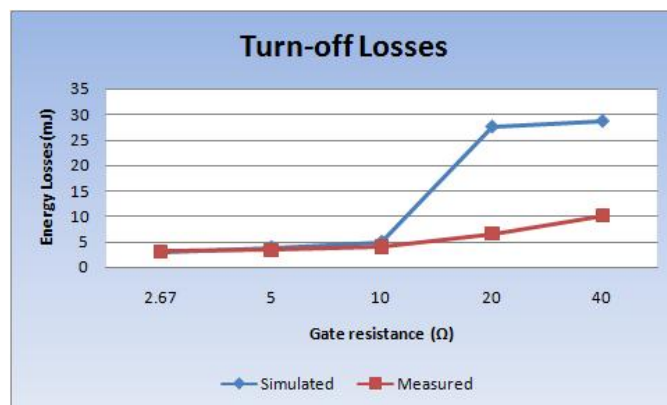


Figure 5.14: Turn-off losses for different gate resistances

From figures 5.13 and 5.14, it can be seen that the turn-on and turn-off losses increase with the gate resistance both for the simulated and for the measured results. This is due to that the gate resistance has a significant impact on the dynamic performance of the IGBTs. The turn-on and turn-off duration increases tremendously

with the gate resistance, which contributes the losses to increase. Furthermore, the differences of the losses between the simulation and hardware measurement are increasing with the gate resistance, especially for  $20\Omega$  and  $40\Omega$ . That's maybe caused by the effects of different gate capacitances and input capacitances in the simulation and hardware.

### Free-wheeling diode

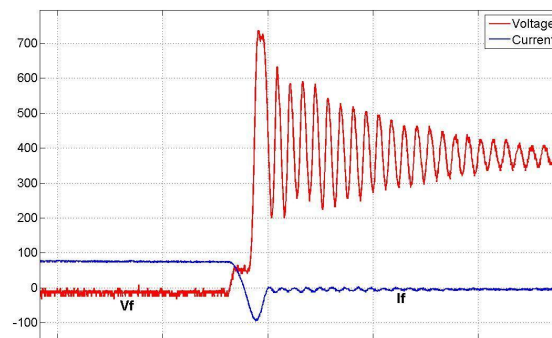


Figure 5.15: Measured diode voltage and current,  $R_g=2.667\Omega$ ,  $0.5\mu s/div$

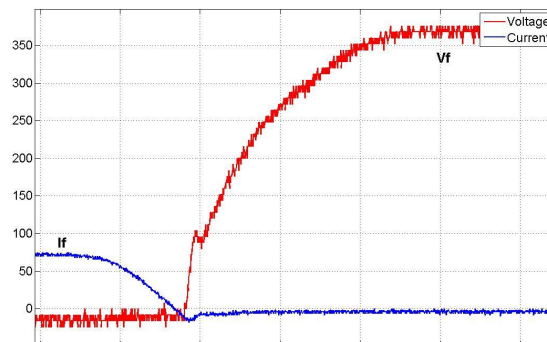


Figure 5.16: Measured diode voltage and current ,  $R_g=40\Omega$ ,  $0.5\mu s/div$

When increases the gate resistance, the current injected into the IGBT gate is

reduced so as to minimize the effects of the reverse recovery current of the free-wheeling diode. So the reverse recovery losses are decreased, as shown in Fig. 5.15 and 5.16. But on the other hand, these effects lead to the overvoltage across the complementary IGBT which is caused by the freewheeling diode snap off and the EMI which is generated by the ringing during the reverse recovery transient.[14]

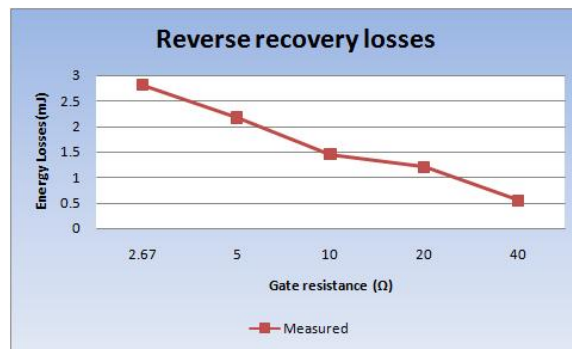


Figure 5.17: Free-wheeling diode reverse recovery losses

The reverse recovery losses decrease with the increase of the gate resistance, shown in Fig. 5.17. With a higher gate resistance, the IGBT turn-on transient is slowed down, hence reducing the value of  $di/dt$  applied to the free-wheeling diode which can reduce the diode losses. However, this is at the expense of increasing the IGBT losses. An alternative approach of reducing the reverse recovery losses is to turn on the IGBT with a reduced  $V_{GE}$  which limits the peak reverse recovery current,  $I_{rr}$ , of the free-wheeling diode. [15]

## 5.5 Effect of current



Figure 5.18: Turn-on losses for different currents



Figure 5.19: Turn-off losses for different currents

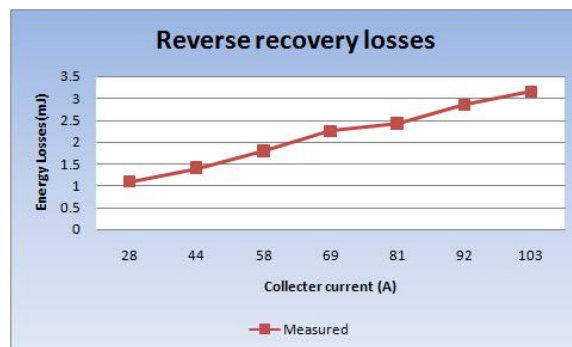


Figure 5.20: Free-wheeling diode reverse recovery losses

It can be seen from Fig. 5.18 and 5.19 that the turn-on and turn-off losses increase with collector current both for the simulated and the measured results. And the simulated losses are much higher than the measured ones at the same current level. That could be due to the different types of free-wheeling diodes that are used in the simulation and hardware. The diode used in the simulation is slower than the real one which is integrated into the IGBT module. In Fig. 5.20, the reverse recovery losses are increasing with the reverse recovery current which is affected by the collector current. The higher of the peak reverse recovery current, the faster the IGBT is switched on.

## 5.6 Effect of temperature

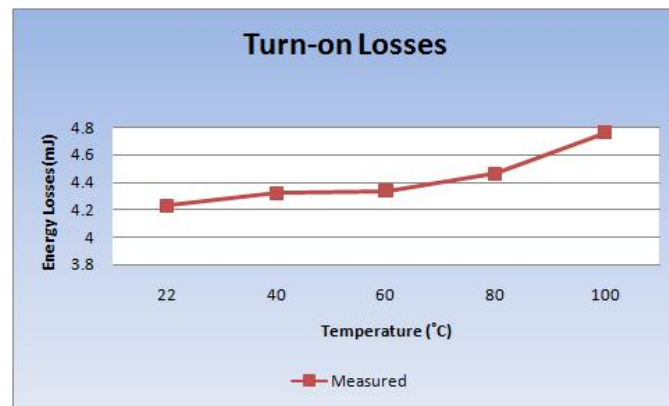


Figure 5.21: *Turn-on losses for different temperatures*

From Fig. 5.21 and 5.22, it can be seen that both the turn-on and turn-off losses are constant with the temperature changes. That is because for this non-punch through IGBT, the turn-off duration remains constant in its working temperature range.

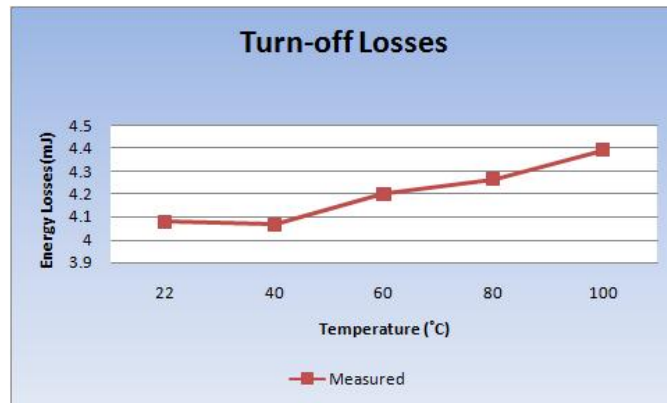


Figure 5.22: Turn-off losses for different temperatures

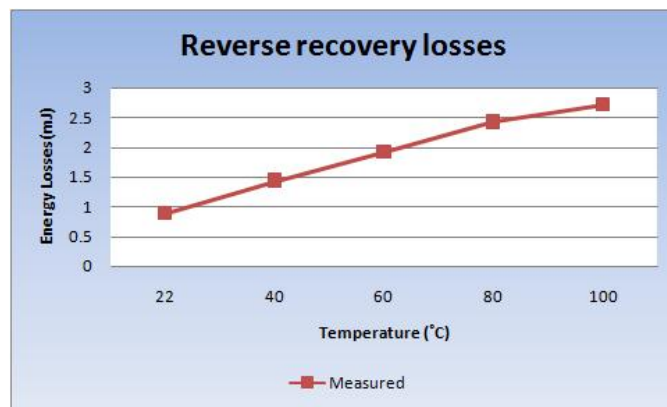


Figure 5.23: Free-wheeling diode reverse recovery losses

For the free-wheeling diode, however, the reverse recovery losses, shown in Fig. 5.23, increase with the temperature. That is due to the reverse recovery current which will increase with the temperature.

# Chapter 6

## Conclusion and outlook

### 6.1 Conclusion

An IGBT test setup is designed and built to investigate the switching characteristics and losses of a new IGBT module CM300DC-24NFM. A specific IGBT control and drive PCB is constructed to provide a high quality IGBT gate signal.

The switching characteristics and switching losses are explored under different parameters both in the hardware and simulation. It can be seen that the switching losses both for the IGBT and the free-wheeling diode are increasing with the voltage and current levels.

The gate resistance also affects the losses greatly: the IGBT switching losses increase with the increase of the gate resistance; on the other hand, the reverse recovery losses decrease with the gate resistance.

In addition, the switching losses of this new IGBT module is not affected so apparently by the temperature variation. The reverse recovery losses, however, increase significantly with the temperature.

The stray inductance affects the switching characteristics remarkably, so it should be as low as possible.

## 6.2 Future work

The IGBT manufacture technology develops fast recent years and even faster in the future. New IGBT modules with higher voltage and current ratings are needed to be investigated thoroughly.

Due to the measurement equipment restrictions, the switching losses are not measured at higher voltage levels ( $>400\text{V}$ ) both for model1 and model 2. This can be realized by using large range voltage differential probes and Rogowishi coils.

The security conditions are also needed to be improved. It is better to put the experimental setup in an insulated metal case to avoid contact with high voltage during the test.

The control circuit can be replaced by micro processor. This can provide a control signal by programming which saves time and cost.

# Bibliography

- [1] MITSUBISHI ELECTRIC. Mitsubishi semiconductors power modules mos introduction. page 2, 1998.
- [2] Anna von Zweigbergk. Förlustkaraktisering av igbt ventiler. Master's thesis, CHALMERS UNIVERSITY OF TECHNOLOGY, 2006.
- [3] Francis Mulolani Xiaoxiao Ni. Measurement of switching transitions in igbts. Master's thesis, CHALMERS UNIVERSITY OF TECHNOLOGY, 2006.
- [4] G. Ledwich. Igbts basics [online]. 1998. Available from: [http://www.powerdesigners.com/InfoWeb/design\\_center/articles/IGBTs/igbts.shtm](http://www.powerdesigners.com/InfoWeb/design_center/articles/IGBTs/igbts.shtm).
- [5] Undeland Mohan and Robbins. *Power Electronics: Converters, Applications and Design*. Wiley, 2003.
- [6] Muhammad H.Rashid. *Power Electronics Handbook*. Academic Press, 2001.
- [7] Marc T. Thompson. Inductance calculation techniques. *Power Control and Intelligent Motion*, 1999.
- [8] Rik W. De Doncker Alberto Tenconi Marco Chiad'O Caponet, Francesco Profumo. Low stray inductance bus bar design and construction for good emc performance in power electronic circuits. *IEEE TRANSACTIONS ON POWER ELECTRONICS*, 17:225–231, 2002.

- [9] Rudy Severns. Design of snubbers for power circuits.
- [10] Tektronix. Differential probes [online]. Available from: [http://www.tek.com/products/accessories/oscilloscope\\_probes/differential.html](http://www.tek.com/products/accessories/oscilloscope_probes/differential.html).
- [11] Altera. Minimizing ground bounce and  $v_{CC}$  sag. November 2001.
- [12] J. La T. Exon D. A. Ward. Using rogowski coils for transient current measurements. *ENGINEERING SCIENCE AND EDUCATION JOURNAL*, page 111, JUNE 1993.
- [13] Y.Seki Y.Onozawa, M.Otsuki. Great improvement in turn-on power dissipation of igbts with an extra gate charging function. *17<sup>th</sup> International Symposium on Power Semiconductor Devices and IC's*, 2005.
- [14] Thomas A. Lipo Vinod John, Bum-Seok Suh. High-performance active gate drive for high-power igbt's. *IEEE TRANSACTIONS ON INDUSTRY APPLICATIONS*, VOL. 35, NO. 5:1110, SEPTEMBER/OCTOBER 1999.
- [15] DYNEX SEMICONDUCTOR. Gate drive considerations for maximum igbt efficiency application note. September 2000.

# Appendix A

## Control and drive circuit schematics

The control and drive PCB schematics blueprint is here.